

Prediction and Experimental Validation Studies of Wet Flue Gas Desulphurization with a Novel Type PCF Device Based on Limestone-Gypsum

Hongliang Gao,^{†,‡} Caiting Li,^{*,†,‡} Guangming Zeng,^{†,‡} Wei Zhang,^{†,‡} Lin Shi,^{†,‡} Shanhong Li,^{†,‡}
Yanan Zeng,[§] Xiaopeng Fan,^{†,‡} Qingbo Wen,^{†,‡} and Xin Shu^{†,‡}

[†]College of Environmental Science and Engineering, Hunan University, Changsha 410082, P. R. China, [‡]Key Laboratory of Environmental Biology and Pollution Control (Hunan University), Ministry of Education, Changsha 410082, P. R. China, and [§]College of Economics, Central South University of Forestry and Technology, Changsha 410004, P. R. China

Received June 29, 2010. Revised Manuscript Received August 12, 2010

A novel wet-type flue gas desulphurization process were developed and tested in this study. The process used a PCF device as the absorber where SO₂ was absorbed into slurry of reactive CaCO₃. A model of external mass-transfer based on the two-film theory was proposed for estimation of the SO₂ absorption in the PCF device, and the theoretical SO₂ removal efficiency was compared with the experimental data. The results show that the SO₂ absorption rate in the spray zone is controlled by a combination of gas- and liquid-film diffusions in the range of tested operating conditions. The increase of gas flow rate and droplet size and decrease of liquid–gas ratio all can lead to a decrease in the SO₂ removal efficiency. Addition of Cl⁻ to the slurry (25 g/L) decreases the SO₂ removal efficiency from 83.87 to 70.75%. when comparing the results of prediction and experiment, the data show good agreement. With droplet size equal to 2500 μm, when gas flow rate and liquid–gas ratio are changed, the relative errors of SO₂ removal efficiency between the predicted and experimental data are below 3.40 and 8.67%, respectively. It demonstrates that the model proposed in the present study is an effective model to evaluate and predict the desulphurization performance of the novel type PCF device. Moreover, the theoretical model can be extended to apply in other wet FGD technologies.

1. Introduction

Combustion of sulfur-containing fossil fuels such as coal and oil results in sulfur dioxide (SO₂) emission. SO₂ is known to have detrimental effects on human health and the environment, and as a consequence receives more and more attention.¹ Several processes have been developed for reducing SO₂ emissions from coal utilization, such as fuel pretreatment, concurrent burning and adsorption, and flue gas post treatment, that is, flue gas desulphurization (FGD).^{2,3} Among these schemes, the wet FGD processes, especially the lime/limestone-gypsum process, have earned widespread use due to high SO₂ removal efficiency and reliability and low utility consumption.⁴

The PCF device is newly developed for industrial application of wet FGD, having sleeve structure. It is derived from the conventional granite water film dust collector (GWFDC) by building an outer cylinder around the original GWFDC. The outer cylinder is lower than inner cylinder (original GWFDC), and between them is a preliminary treating chamber where gas and liquid contact and are in coflows. Self-excitation channels lying in the wall of the inner cylinder are employed to connect the preliminary treating chamber and inner cylinder and to

simultaneously make the gas rotate into the inner cylinder. At the bottom of the inner cylinder is a self-excitation chamber that has second purification for the flue gas. The whole inner cylinder is used to remove water from air. Compared with the original GWFDC, the novel wet-type PCF device possesses the following virtues: (a) Dewatering performance improves significantly, and an extra demister is out of consideration. No demister means lower energy-consumption, cost, and maintenance. (b) There are co-flows of gas and liquid in the preliminary treating chamber and no venturi structure in the inlet tube, therefore the pressure drop of the device is much lower than that of the original GWFDC. (c) The self-excitation chamber has a second purification for the flue gas, which further improves the collection efficiency of the device. (d) Draft fans of the original GWFDC can be used in the novel PCF device, reducing the investment cost of the PCF desulphurization technology.

Some studies have been carried out to describe and predict the wet FGD process such as notable those by Olausson et al.,⁵ Lancia et al.,⁶ Frandsen et al.,⁷ and Kiil et al.⁸ These models are usually complicated and feature a detailed description of the chemistry including SO₂ absorption and oxidation, limestone dissolution, and gypsum precipitation. They also gave the estimation of desulphurization efficiency and investigated the influence of some operating parameters such as the

*To whom correspondence should be addressed. Phone: +86 731 88649216. Fax: +86 731 88649216. E-mail: cqli@hnu.cn, ghliang007@163.com.

(1) Marocco, L.; Inzoli, F. *Int. J. Multiphas. Flow* **2009**, *35*, 185–194.
(2) Dou, B. L.; Byun, Y. C.; Hwang, J. G.. *Energy Fuels* **2008**, *22*, 1041–1045.

(3) Un, U. T.; Koparal, A. S.; Ögütveren, U. B. *Sep. Purif. Technol.* **2007**, *53*, 57–63.

(4) Gutierrez Ortiz, F. J.; Vidal, F.; Ollero, P.; Salvador, L.; Cortes, V.; Gimenez, A. *Ind. Eng. Chem. Res.* **2006**, *45*, 1466–1477.

(5) Olausson, S.; Wallin, M.; Bjerle, I. *Chem. Eng. J.* **1993**, *51*, 99–108.
(6) Lancia, A.; Musmarra, D.; Pepe, F. *Ind. Eng. Chem. Res.* **1997**, *36*, 197–203.

(7) Frandsen, J. B. W.; Kiil, S.; Johnsson, J. E. *Chem. Eng. Sci.* **2001**, *56*, 3275–3287.

(8) Kiil, S.; Nygaard, H.; Johnsson, J. E. *Chem. Eng. Sci.* **2002**, *57*, 347–354.

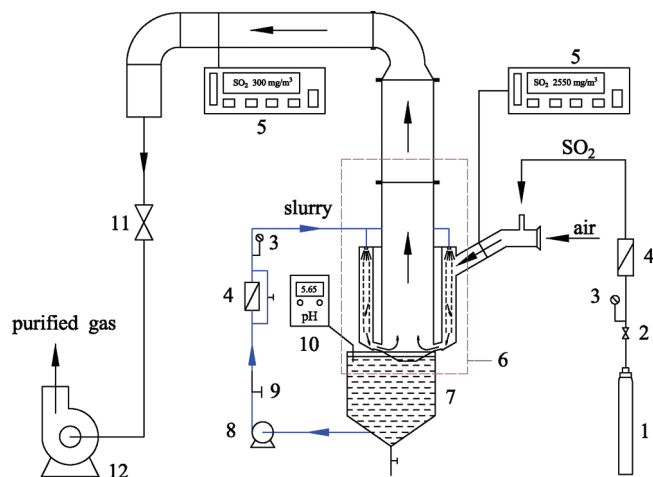


Figure 1. Schematic diagram of the experimental setup: (1) bottled SO₂; (2) pressure reduction valve; (3) manometer; (4) rotameter; (5) SO₂ analyzer; (6) absorber; (7) slurry tank; (8) slurry pump; (9) valve; (10) pH meter; (11) volume damper; (12) exhaust fan.

liquid–gas ratio, slurry-droplet size, and concentration of HCl or the effect of adding organic acids. Brogren and Karlsson⁹ developed a model based on the penetration theory to calculate the dynamic absorption rate of SO₂ into the limestone slurry droplet. The model elucidated various facets of reactions with a finite rate. Muginstein et al.¹⁰ developed a model relevant to spray towers for gas absorption into a large slurry droplet, with the results indicating that internal circulation enhanced the mass-transfer with respect to a stagnant droplet for large droplets. Scala and D'Ascenzo¹¹ developed a model for gas absorption via an instantaneous reaction in a droplet. Wang et al.¹² found that the spray water flow rate and the droplet's size had an obvious influence on the SO₂ removal efficiency. Bandyopadhyay and Biswas¹³ predicted the removal efficiency of a novel two-stage hybrid scrubber for flue gas desulfurization. Dou and Hwang² proposed a simple prediction of SO₂ removal with Ca(OH)₂ slurry for semidry FGD process used an electrostatic spraying absorber (ESA) as the reactor. However, as far as the study on the novel type PCF device is concerned, very little work has been reported on its performance through a theoretical model. Therefore, the objective of this work was to develop a theory model of SO₂ absorption into limestone slurry droplets based on the two-film mass-transfer theory and use the model to predict the SO₂ removal efficiency and quantify the mass-transfer resistances within the novel type PCF device. Meanwhile, some auxiliary experiments were conducted to validate the predicted results.

2. Experimental Section

A schematic diagram of the experimental setup is shown in Figure 1, of which the essential element is the absorber (6) where SO₂ removal occurs. The desired amount of SO₂ in air was prepared by mixing bottled SO₂ (1) with air drafted by the exhaust fan (12). Volumetric flow rates of SO₂ and air were adjusted by the pressure reduction valve (2) and volume damper (11), respectively. SO₂ was absorbed by limestone slurry. Limestone slurry

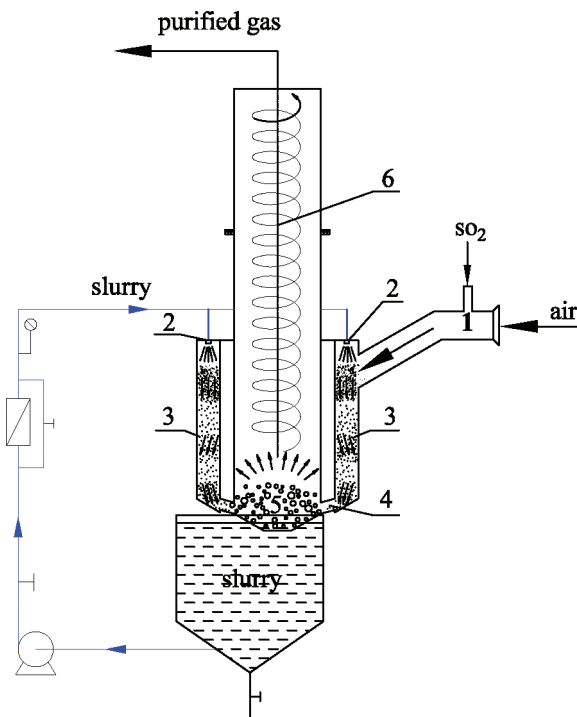


Figure 2. PCF device as absorber: (1) inlet tube; (2) nozzle; (3) preliminary treating chamber; (4) self-excitation channel; (5) self-excitation chamber; (6) inner cylinder.

was prepared by mixing CaCO₃ of 25 μm with tap water was stored in a slurry tank (7). The circulating pump (8) was provided for the recirculation of the limestone slurry, and the quantity of the slurry pumped into the absorber was adjusted by means of a valve (9). During the experiment, a digital pH meter (Model: HI 8424) (10) was employed to measure the pH value of slurry by inserting a pH probe into the liquid phase. A pitot tube (model: Y25–150) was used to measure the gas flow rate, and two micro-computer smoke test instruments (model: Leibo3020) (5) were employed for online measurement of SO₂ concentration in gas phase by putting sensors at the test cross sections of the inlet tube and the outlet tube simultaneously.

The absorber used in this study is a lab-scale PCF device, as shown in Figure 2. It consists of a preliminary treating chamber (3) and an inner cylinder (6). The air–SO₂ mixture first enters the preliminary treating chamber through the inlet tube (1) at the side-top of the absorber. The preliminary treating chamber is an annular configuration with a width of 0.08 m and a height of 0.565 m. At the top of it, nozzles (2) are distributed and generate atomization. When the gas passes through the preliminary treating chamber, SO₂ gets preliminary purification by reacting with CaCO₃ in the absorbing liquid. Then, the gas goes through the self-excitation channels (4) and enters the inner cylinder (6). The inner cylinder is a cylinder with a diameter of 0.3 m and a height of 1.4 m. At the bottom of it, there is a conical self-excitation chamber (5) where the rotary gas from self-excitation channels can impinge the liquid in slurry tank, and consequently lots of bubbles are produced, improving the secondary-purification effect for the gas. As the gas swirls up, water is removed from the air and the purified gas is released to the atmosphere through the exhaust tube. The scrubbed liquid flows into the inner cylinder along with self-excitation channels and returns to the recycle slurry tank.

The experiments were carried out in a batch mode. Before each run, the tank was refilled with fresh limestone slurry. The data were collected during the first 3–4 min. Because the slurry volume was about 450 L and the slurry pump capacity was equal to 100 L/min, the slurry was recycled only almost one time during 3–4 min runs.

(9) Brogren, C.; Hans, T. K. *Chem. Eng. Sci.* **1997**, *52*, 3085–3099.

(10) Muginstein, A.; Fichman, M.; Gutfinger, C. *Int. J. Multiphase Flow* **2001**, *27*, 1079–1094.

(11) Scala, F.; D'Ascenzo, M. *AIChE J.* **2002**, *48* (8), 1719–1726.

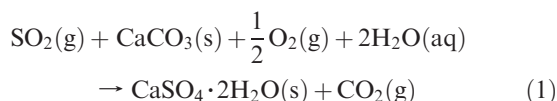
(12) Wang, L.; Song, Y. B.; Zhang, M. C.; Fan, H. J.; Zhou, Y. G.; Fan, W. D.; Wu, J. *Chem. Eng. Sci.* **2005**, *60* (4), 951–962.

(13) Bandyopadhyay, A.; Biswas, M. N. *Chem. Eng. Technol.* **2006**, *29* (1), 130–145.

Thus, SO₂ concentration in slurry did not increase significantly. The addition of Cl⁻ was added to the slurry tank in the form of CaCl₂ (s) in the experiment.

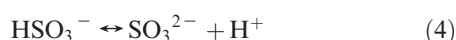
3. Modeling

In the wet limestone desulphurization system, a complex series of kinetic and equilibrium controlled by reactions occur in the gas, liquid, and solid phases. The overall reaction can be written as:

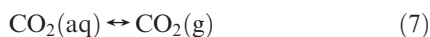
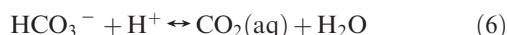


Five steps are included in the above reaction: absorption, neutralization, regeneration, oxidation and precipitation, all of which occur simultaneously in the process.¹

(1) Absorption



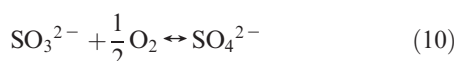
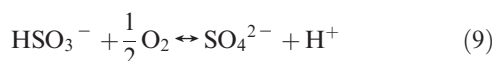
(2) Neutralization



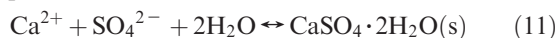
(3) Regeneration



(4) Oxidation



(5) Precipitation



As far as the novel type PCF device is concerned, SO₂ absorption mainly takes place in the preliminary treating chamber (spray zone) and self-excitation chamber. As a consequence, the theoretical model of SO₂ absorption for the PCF device only considered these two aspects in present study. Some simplified assumptions were given as follows:^{9,13–16} (1) The Henry's law is applicable for SO₂; (2) The reactions between two species are instantaneous and at equilibrium; (3) The droplet is spherical; (4) There is no resistance at the gas–liquid phase interface; (5) Reactions of regeneration, oxidation, and precipitation only occur in the slurry tank; (6) Heats of reaction and dissolution can be neglected, and the system is isothermal.

3.1. Modeling of SO₂ Absorption in the Preliminary Treating Chamber. Flue gas is treated as the studied object. The

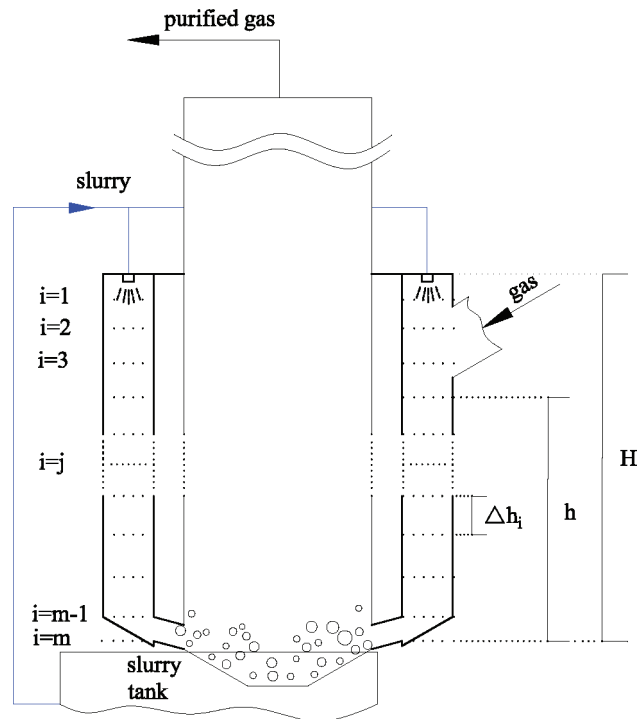


Figure 3. Division scheme of the preliminary treating chamber into layers.

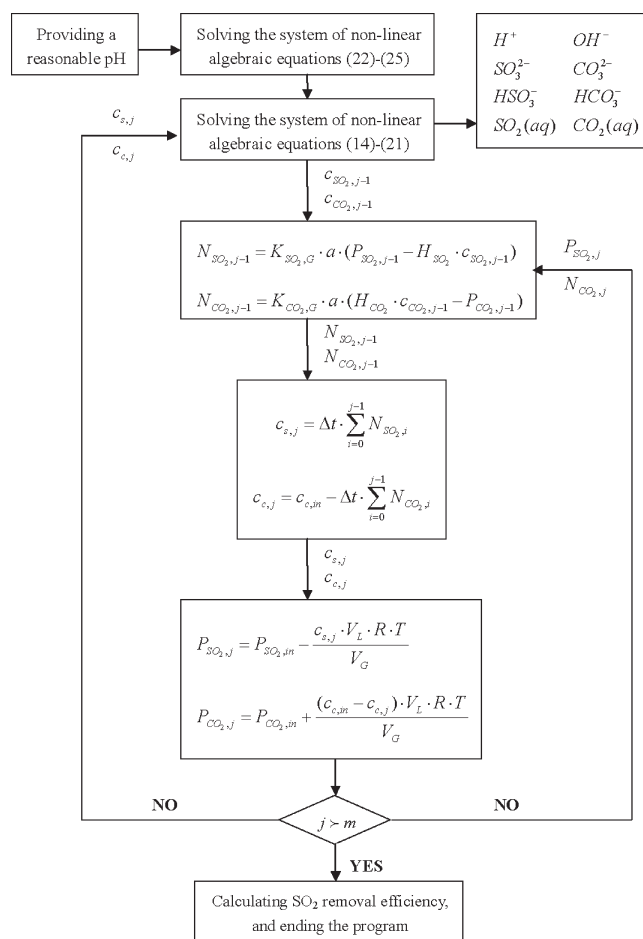


Figure 4. Framework map of SO₂ absorption model for the preliminary treating chamber.

(14) Ramachandran, P. A.; Sharma, M. M. *Chem. Eng. Sci.* **1969**, *24*, 1681–1686.

(15) Liu, S.; Xiao, W. *Chem. Eng. Technol.* **2006**, *29*, 1167–1173.

(16) Warych, J.; Szymanowski, M. *Ind. Eng. Chem. Res.* **2001**, *40*, 2597–2605.

average residence time of gas in preliminary treating chamber, t , is first determined by the following equation:

$$t = \xi \frac{V_R}{V_G} \quad (12)$$

where V_G and V_R are the gas flow rate and preliminary treating chamber volume, respectively; and ξ is a correction factor, illustrating the effect of reactor type on the residence time of gas.

Then the residence time is averagely divided into m parts. As a result, the preliminary treating chamber can be divided into m layers in accordance with the time step size, as shown in Figure 3. The time step size, Δt , is defined as

$$\Delta t = \frac{t}{m} \quad (13)$$

It is assumed that the composition of droplets and absorption rate of SO_2 remain unchanged in a time step size. Thus, the gas–liquid mass-transfer in the preliminary treating chamber can be studied in each layer. The detailed information is illustrated in Figure 4.

The first step is to determine the concentrations of $\text{SO}_2(\text{aq})$ and $\text{CO}_2(\text{aq})$ by analyzing the aqueous phase chemistry. According to the assumptions, only reactions 2–7 are analyzed in the preliminary treating chamber. These equilibrium reactions 3–6, together with water dissociation, electroneutrality, and mass balances of the carbon species and sulfur species, form a system of nonlinear algebraic equations, 14–21. Chloride ion (Cl^-), calcium ion (Ca^{2+}), and eight dissolved species (H^+ , OH^- , $\text{SO}_2(\text{aq})$, $\text{CO}_2(\text{aq})$, HSO_3^- , HCO_3^- , SO_3^{2-} , and CO_3^{2-}) are considered to define the liquid phase composition.

$$K_{S1} = \frac{[\text{HSO}_3^-][\text{H}^+]}{[\text{SO}_2(\text{aq})]} \quad (14)$$

$$K_{S2} = \frac{[\text{SO}_3^{2-}][\text{H}^+]}{[\text{HSO}_3^-]} \quad (15)$$

$$K_{C1} = \frac{[\text{HCO}_3^-][\text{H}^+]}{[\text{CO}_2(\text{aq})]} \quad (16)$$

$$K_{C2} = \frac{[\text{CO}_3^{2-}][\text{H}^+]}{[\text{HCO}_3^-]} \quad (17)$$

$$K_{\text{H}_2\text{O}} = [\text{H}^+][\text{OH}^-] \quad (18)$$

$$[\text{H}^+] + 2[\text{Ca}^{2+}] = [\text{OH}^-] + [\text{HSO}_3^-] + [\text{HCO}_3^-] + 2[\text{SO}_3^{2-}] + 2[\text{CO}_3^{2-}] + [\text{Cl}^-] \quad (19)$$

$$c_c = [\text{CO}_2(\text{aq})] + [\text{HCO}_3^-] + [\text{CO}_3^{2-}] \quad (20)$$

$$c_s = [\text{SO}_2(\text{aq})] + [\text{HSO}_3^-] + [\text{SO}_3^{2-}] \quad (21)$$

The concentration of Cl^- is an input parameter, $[\text{Ca}^{2+}]$ in a falling droplet is unchanged and is equal to the $[\text{Ca}^{2+}]$ in the slurry tank because the limestone dissolution is neglected in the preliminary treating chamber, and concentrations of eight kinds of dissolved species are obtained at each time period by solving the system of nonlinear algebraic eqs 14–21.

At the beginning of the calculation, the composition of droplets into the preliminary treating chamber is identical to

that of the fresh slurry. $[\text{SO}_2(\text{aq})]$, $[\text{HSO}_3^-]$ and $[\text{SO}_3^{2-}]$ are equal to 0; $[\text{H}^+]$ and $[\text{OH}^-]$ are determined by the given slurry pH value depending on process and economical considerations; and $[\text{Ca}^{2+}]$, $[\text{CO}_2(\text{aq})]$, $[\text{HCO}_3^-]$, and $[\text{CO}_3^{2-}]$ are calculated by the system of chemical reactions 22–24 and electroneutrality 25 in slurry tank.

$$K_{\text{CaCO}_3} = [\text{Ca}^{2+}][\text{CO}_3^{2-}] \quad (22)$$

$$K_{C1} = \frac{[\text{HCO}_3^-][\text{H}^+]}{[\text{CO}_2(\text{aq})]} \quad (23)$$

$$K_{C2} = \frac{[\text{CO}_3^{2-}][\text{H}^+]}{[\text{HCO}_3^-]} \quad (24)$$

$$[\text{H}^+] + 2[\text{Ca}^{2+}] = [\text{OH}^-] + [\text{HCO}_3^-] + 2[\text{CO}_3^{2-}] + [\text{Cl}^-] \quad (25)$$

After the concentrations of $\text{SO}_2(\text{aq})$ and $\text{CO}_2(\text{aq})$ are determined, the next step is to calculate the gas–liquid mass-transfer rate. Equations 2 and 7 demonstrate the absorption of SO_2 into liquid phase and desorption of CO_2 into gas phase, respectively. To describe the process, the two-film mass-transfer theory is employed in present study, and the absorption rate of SO_2 and desorption rate of CO_2 in preliminary treating chamber are expressed as¹⁷

$$N_{\text{SO}_2} = K_{\text{SO}_2, G} a (P_{\text{SO}_2} - H_{\text{SO}_2} c_{\text{SO}_2}) \quad (26)$$

$$N_{\text{CO}_2} = K_{\text{CO}_2, G} a (H_{\text{CO}_2} c_{\text{CO}_2} - P_{\text{CO}_2}) \quad (27)$$

where P_{SO_2} and P_{CO_2} are the partial pressures of SO_2 and CO_2 in gas phase (Pa), c_{SO_2} and c_{CO_2} are the concentrations of SO_2 and CO_2 in liquid phase (mol/m^3), and, $K_{\text{SO}_2, G}$ and $K_{\text{CO}_2, G}$ are the overall mass-transfer coefficients of SO_2 and CO_2 ($\text{mol}/\text{m}^2 \cdot \text{s} \cdot \text{Pa}$), calculated by

$$\frac{1}{K_{\text{SO}_2, G}} = \frac{1}{k_{\text{SO}_2, G}} + \frac{H_{\text{SO}_2}}{E_{\text{SO}_2} k_{\text{SO}_2, L}} \quad (28)$$

$$\frac{1}{K_{\text{CO}_2, G}} = \frac{1}{k_{\text{CO}_2, G}} + \frac{H_{\text{CO}_2}}{k_{\text{CO}_2, L}} \quad (29)$$

where $k_{\text{SO}_2, G}$ and $k_{\text{CO}_2, G}$ are the gas-side mass-transfer coefficients of SO_2 and CO_2 ($\text{mol}/\text{m}^2 \cdot \text{s} \cdot \text{Pa}$), $k_{\text{SO}_2, L}$ and $k_{\text{CO}_2, L}$ are the liquid-side mass-transfer coefficients of SO_2 and CO_2 (m/s), H_{SO_2} and H_{CO_2} are the Henry's constants of SO_2 and CO_2 ($\text{m}^3 \cdot \text{Pa}/\text{mol}$), and E_{SO_2} is the mass-transfer enhancement factor of SO_2 for instantaneous chemical reaction, given as^{18,19}

$$E_{\text{SO}_2} = 1 + \xi \frac{D_{\text{CaCO}_3} c_{\text{CaCO}_3}}{D_{\text{SO}_2, L} c_{\text{SO}_2}} \quad (30)$$

where D_{CaCO_3} is the diffusion coefficient of CaCO_3 in liquid phase (m^2/s), $D_{\text{SO}_2, L}$ is the diffusion coefficient of SO_2 in liquid phase (m^2/s), c_{CaCO_3} is the concentration of CaCO_3 in liquid phase (mol/m^3), and ξ is the molar ratio of SO_2 to

(17) Gerbec, M.; Stergarsek, A.; Kocjancic, R. *Comput. Chem. Eng.* **1995**, *19*, s283–s286.

(18) Dou, B. L.; Pan, W. G.; Jin, Q.; Wang, W. H.; Li, Y. *Energ. Convers. Manage.* **2009**, *50*, 2547–2553.

(19) Lin, C.; Zhang, J. Y. *Enhancement factor of gas absorption in gas-liquid-solid three-phase reaction system accompanied by solid dissolution [C]* // *Advances in Separation Science and Technology*; China Environmental Science Press: Beijing, 1998; pp 606–610.

limestone reagent (mol/mol). Actually, E_{SO_2} should be drawn versus the spray height and compared with other numerical or experimental works.⁸ To simplify the calculation in present study, the value of enhancement factor is replaced with an average.²

The specific gas–liquid interface area, a , is defined as²

$$a = \frac{6}{d_p} \quad (31)$$

where d_p is the average size of slurry droplets (m).

As there is no sulfur species at the injection of droplets, the dissolved sulfur species in the falling droplets are produced by the absorbed SO_2 . Their total concentration during the corresponding layer is equal to the combination of a time step size and accumulated absorption rate.

$$c_{s,j} = \Delta t \sum_{i=0}^{j-1} N_{\text{SO}_2,i} \quad (32)$$

While the dissolved carbon species in falling droplets during the corresponding layer is calculated by

$$c_{c,j} = c_{c,\text{in}} - \Delta t \sum_{i=0}^{j-1} N_{\text{CO}_2,i} \quad (33)$$

where $c_{c,\text{in}}$ is the dissolved carbon species in slurry tank (mol/m^3). By virtue of eqs 34 and 35, the SO_2 and CO_2 partial pressure in gas phase can be obtained.

$$P_{\text{SO}_2,j} = P_{\text{SO}_2,\text{in}} - \frac{c_{s,j} \cdot V_L \cdot R \cdot T}{V_G} \quad (34)$$

$$P_{\text{CO}_2,j} = P_{\text{CO}_2,\text{in}} + \frac{(c_{c,\text{in}} - c_{c,j}) \cdot V_L \cdot R \cdot T}{V_G} \quad (35)$$

where $P_{\text{SO}_2,\text{in}}$ and $P_{\text{SO}_2,j}$ are the SO_2 partial pressure in the gas phase at inlet and a given layer inside the preliminary treating chamber, respectively; $P_{\text{CO}_2,\text{in}}$ and $P_{\text{CO}_2,j}$ are the CO_2 partial pressure in the gas phase at inlet and a given layer inside the preliminary treating chamber, respectively; V_L is the slurry flow rate (m^3/s).

Thus, the SO_2 removal efficiency at a given layer inside the preliminary treating chamber is defined as

$$\eta_{\text{pre},j} = 1 - \frac{P_{\text{SO}_2,j}}{P_{\text{SO}_2,\text{in}}} \quad (36)$$

By repeating the preceding steps, more SO_2 removal efficiency results for all layers can be obtained.

As to the solution to the system of nonlinear algebraic eqs 14–21 and 22–25, it was obtained with the globally convergent Newton–Raphson method, as described by Dennis and Schnabel.²⁰ The criterion for stopping the calculation is defined as 1.0×10^{-9} . The whole process of calculation was achieved by virtue of a computational program.

3.2. Modeling of SO_2 Absorption in the Self-Excitation Chamber. The bubbles impinged by the rotary gas from the self-excitation channels play an important role in SO_2 absorption in this zone. The gas–liquid mass-transfer was also based on the two-film theory. The mass-transfer rate of SO_2 is expressed as

$$N_{\text{SO}_2}' = K_{\text{SO}_2,G'} a' (P_{\text{SO}_2,\text{m}} - H_{\text{SO}_2} \cdot c_{\text{SO}_2,\text{m}}) \quad (37)$$

Table 1. Parameters for the PCF Desulphurization System

parameter	value
temperature of gas	atmosphere (25 ± 1 °C)
operating pressure	atmosphere
limestone content in feed stream (wt %)	10
limestone slurry pH	5.7 ± 0.1
volume fraction of CO_2 in the air (%)	0.03
SO_2 inlet concentration (g/m^3)	2.5
slurry concentration of Cl^- (g/m^3)	0
gas flow rate (m^3/s)	0.24
liquid–gas ratio (L/m^3)	10
droplet size (μm)	2500
D_{CaCO_3} (m^2/s)	1.6×10^{-9}
$D_{\text{SO}_2,\text{G}}$ (m^2/s)	1.4×10^{-5}
$D_{\text{SO}_2,\text{L}}$ (m^2/s)	1.8×10^{-9}
$D_{\text{CO}_2,\text{G}}$ (m^2/s)	1.5459×10^{-5}
$D_{\text{CO}_2,\text{L}}$ (m^2/s)	2.2431×10^{-5}
H_{SO_2} ($\text{m}^3 \cdot \text{Pa}/\text{mol}$)	81.06
H_{CO_2} ($\text{m}^3 \cdot \text{Pa}/\text{mol}$)	2851.81
σ (N/m)	7.2×10^{-2}
μ_G ($\text{Pa} \cdot \text{s}$)	1.7894×10^{-5}

where $K_{\text{SO}_2,G'}$ is the overall mass-transfer coefficient of SO_2 in self-excitation chamber ($\text{mol}/\text{m}^2 \cdot \text{s} \cdot \text{Pa}$), $P_{\text{SO}_2,\text{m}}$ is the SO_2 partial pressure in gas phase at the outlet of self-excitation channels (Pa), and $c_{\text{SO}_2,\text{m}}$ is the SO_2 concentration in slurry at the surface of slurry tank (mol/m^3). a' is the effective gas–liquid interface area of self-excitation chamber (m^2), calculated by

$$a' = \frac{6}{d_b} V x_v \quad (38)$$

where d_b is the average size of bubbles (m), measured by the PIV experiment; V is the volume of space stuff with bubbles (m^3); x_v is the volume fraction of bubbles in the V volume.

When N_{SO_2}' is introduced into the eq 39, the SO_2 partial pressure in gas phase at outlet, $P_{\text{SO}_2,\text{out}}$, can be obtained.

$$(P_{\text{SO}_2,\text{m}} - P_{\text{SO}_2,\text{out}}) V_G = N_{\text{SO}_2}' R T \quad (39)$$

Thus, the SO_2 removal efficiency in self-excitation chamber is given as

$$\eta_{\text{self}} = 1 - \frac{P_{\text{SO}_2,\text{out}}}{P_{\text{SO}_2,\text{m}}} \quad (40)$$

Combining the purifications of preliminary treating chamber and self-excitation chamber for the flue gas, the overall SO_2 removal efficiency of the PCF device is defined as

$$\eta_{\text{overall}} = 1 - (1 - \eta_{\text{pre}})(1 - \eta_{\text{self}}) \quad (41)$$

4. Results and Discussion

The performance of a FGD system is related to a wide range of variables including $P_{\text{SO}_2,\text{in}}$, c_{CaCO_3} , V_L , V_G , pH, d_p , liquid–gas ratio (V_L/V_G), V_R , Cl^- , etc. Considering a practical process, V_R is first fixed as a design parameter, $P_{\text{SO}_2,\text{in}}$ and c_{CaCO_3} almost keep constant, and the pH is generally selected as 5.7 ± 1 . Thus, the variables of V_L , V_G , d_p , V_L/V_G , and Cl^- may be important and hence are discussed in the following sections. Table 1 presents the basic experimental and simulative parameters for the PCF desulphurization system.

4.1. Interpretation of Mass-Transfer Coefficient. Considering that the mass-transfer theories of SO_2 and CO_2 are basically identical, only the mass-transfer coefficients of SO_2 are interpreted in this section. According to the Frossling correlation,¹⁶ the gas-side mass-transfer coefficient of SO_2 , $k_{\text{SO}_2,\text{G}}$,

(20) Dennis, J. E.; Schnabel, R. B. *Numerical Methods for Unconstrained Optimization and Nonlinear Equations*; Prentice-Hall: Englewood Cliffs, NJ, 1983.

Table 2. Calculated Mass-Transfer Coefficients for Different Droplet Sizes

d_p (μm)	1500	2000	2500	3000
k_G ($\text{mol}/\text{m}^2 \cdot \text{s} \cdot \text{Pa}$)	5.402×10^{-5}	4.591×10^{-5}	4.053×10^{-5}	3.664×10^{-5}
k_L (m/s)	5.093×10^{-4}	4.104×10^{-4}	3.472×10^{-4}	3.028×10^{-4}
K_G ($\text{mol}/\text{m}^2 \cdot \text{s} \cdot \text{Pa}$)	8.231×10^{-6}	6.686×10^{-6}	5.691×10^{-6}	4.988×10^{-6}

was obtained by

$$\text{Sh} = \frac{k_{\text{SO}_2, \text{G}} d_p RT}{D_{\text{SO}_2, \text{G}}} = 2 + 0.6 \text{Re}^{1/2} \text{Sc}^{1/3} \quad (42)$$

where $D_{\text{SO}_2, \text{G}}$ is the diffusion coefficient of SO_2 in gas phase (m^2/s); Sh, Re, and Sc are the Sherwood number, Reynolds number, and Schmidt number, respectively; Re is calculated by eq 43, and Sc is calculated by eq 44.

$$\text{Re} = \frac{\rho_G d_p |u_G - u_p|}{\mu_G} \quad (43)$$

$$\text{Sc} = \frac{\mu_G}{\rho_G D_{\text{SO}_2, \text{G}}} \quad (44)$$

where ρ_G is the gas density (kg/m^3), u_G is the gas velocity (m/s), μ_G is the gas dynamics viscosity ($\text{kg}/\text{m} \cdot \text{s}$), and u_p is the average droplet's velocity (m/s).

The liquid-side mass-transfer coefficient of SO_2 , $k_{\text{SO}_2, \text{L}}$, is estimated by¹⁶

$$k_{\text{SO}_2, \text{L}} = 0.88 \sqrt{\sqrt{\frac{8\sigma}{3\pi m_p}} D_{\text{SO}_2, \text{L}}} \quad (45)$$

where σ is the surface tension of liquid (N/m), and m_p is the mass of a droplet (kg).

Table 2 shows the effect of droplet size on the mass-transfer coefficients of SO_2 in spray zone (preliminary treating chamber), with both the gas- and liquid-side mass-transfer coefficients gradually decreasing with increasing droplet size. Provided that the gas- and liquid-side mass-transfer resistances are defined as $1/k_{\text{SO}_2, \text{G}}$ and $H_{\text{SO}_2}/(E_{\text{SO}_2} k_{\text{SO}_2, \text{L}})$, respectively, the estimation of which phase controls the mass-transfer can be ascribed to the ratio of gas-side resistance to the total mass-transfer resistance, $(1/k_{\text{SO}_2, \text{G}})/(1/K_{\text{SO}_2, \text{G}})$. If $1/k_{\text{SO}_2, \text{G}}$ is nearly equal to $1/K_{\text{SO}_2, \text{G}}$, the mass-transfer is gas phase control, and a ratio of $(1/k_{\text{SO}_2, \text{G}})/(1/K_{\text{SO}_2, \text{G}}) \leq 0.1$ is the criterion for liquid phase control.¹⁸ According to Table 2, it can be calculated that the ratios of $(1/k_{\text{SO}_2, \text{G}})/(1/K_{\text{SO}_2, \text{G}})$ are 0.1524, 0.1457, 0.1404, and 0.1362 for droplet sizes of 1500, 2000, 2500, and 3000 μm , respectively, indicating that both gas- and liquid-side resistances are important, with the absorption rate likely to be controlled by a combination of gas- and liquid-film diffusion controls. The reduction in either side resistance can result in an increasing of SO_2 removal. On the other hand, the calculations show that the ratio of $(1/k_{\text{SO}_2, \text{G}})/(1/K_{\text{SO}_2, \text{G}})$ is slightly bigger than 0.1, which also can be concluded that the absorption of SO_2 into the limestone slurry to a large extent is liquid-side controlled. The conclusion agrees with that of Brogren and Karlsson.⁹

4.2. Predicted Results and Analysis. Provided that the absorption driving force, Δp_{SO_2} , was defined as follows:⁶

$$\Delta p_{\text{SO}_2} = p_{\text{SO}_2} - H_{\text{SO}_2} c_{\text{SO}_2} \quad (46)$$

Figure 5 shows the relationship between absorption rate and driving force at various gas flow rates (a), liquid–gas ratios (b), and droplet sizes (c). As shown in the figures, the absorption rate is in direct proportion to the driving force in the range of

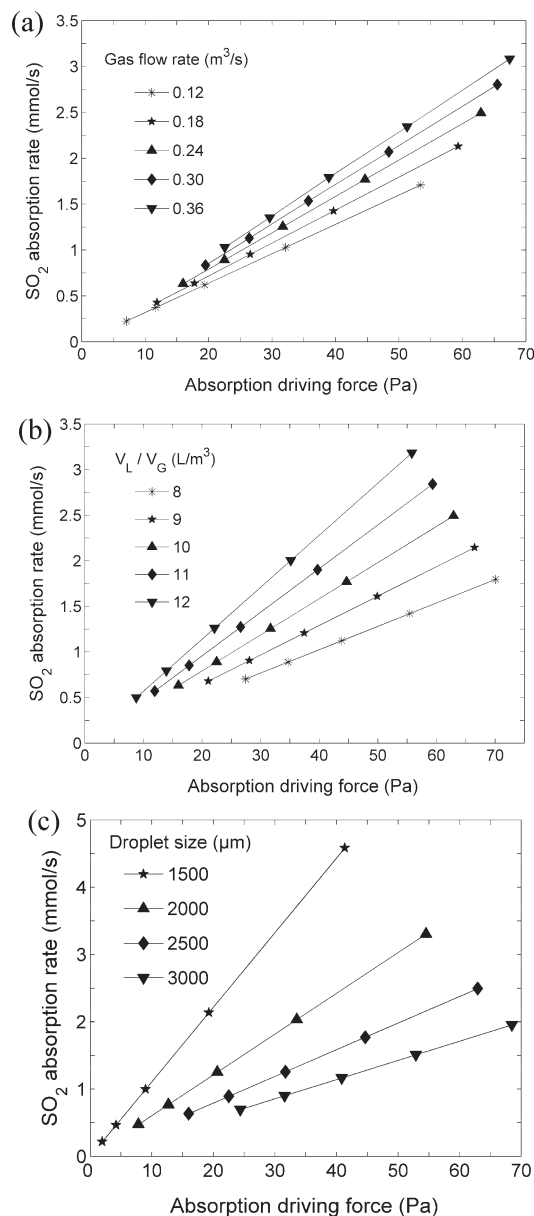


Figure 5. Relationship between absorption rate and absorption driving force at various gas flow rates (a), liquid–gas ratios (b), and droplet sizes (c).

tested operating conditions. The predicted points can be approximated by linear functions passing through the origin of the coordinate system. The correlation coefficient for all straight lines is close to one, $R^2 = 0.999$, which testifies to a very good correlation. The obtained linear relationships testify to the fact that with the increase of the driving force of the absorption process, the value of the mass-transfer coefficient does not change with SO_2 partial pressure. These results agree well with that of Bokotko and Hupka.²¹ Furthermore, the

(21) Bokotko, R. P.; Hupka, J.; Miller, J. D. *Environ. Sci. Technol.* 2005, 39, 1184–1189.

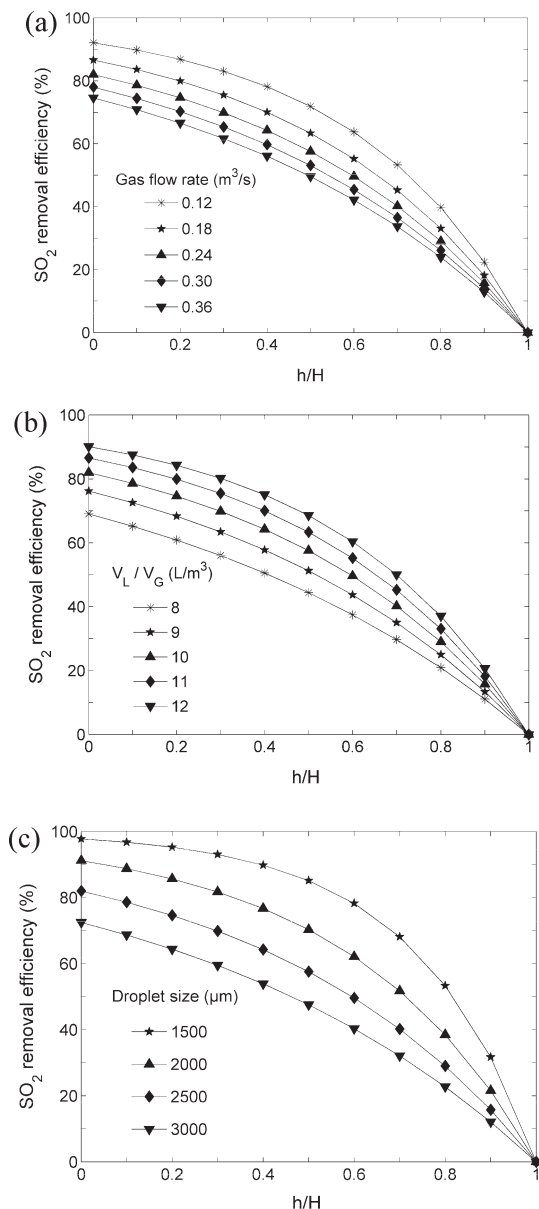


Figure 6. SO₂ removal efficiency at various height of the preliminary treating chamber for different gas flow rates (a), liquid–gas ratios (b), and droplet sizes (c).

increase of gas flow rate and liquid–gas ratio increase the SO₂ absorption rate, while the increase of droplet size decreases it.

Figure 6 gives the SO₂ removal efficiency at various height of the preliminary treating chamber for different gas flow rates (a), liquid–gas ratios (b), and droplet sizes (c). From the figures, it can be seen that SO₂ gets removed as the flue gas moves down in the preliminary treating chamber. The gas flow rate, liquid–gas ratio and droplet size all affect, to various extents, the degree of SO₂ removal. When the gas flow rate is increased, the SO₂ removal efficiency decreases. The possible reason is that the residence time of gas in the preliminary treating chamber becomes shorter during the course. But this does not mean the SO₂ absorption rate decreases. On the contrary, the absorption rate is increased, as seen in Figure 5a. The increase of the liquid–gas ratio leads to an increase in the gas–liquid interface and thereby in the degree of desulphurization. Furthermore, when the gas flow rate and liquid–gas ratio are kept constant, both the

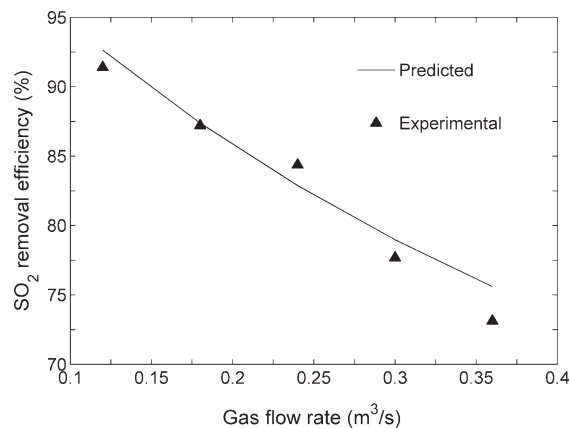


Figure 7. Comparison of SO₂ removal efficiency for different gas flow rates.

specific gas–liquid surface area defined by eq 31 and mass-transfer coefficients increase with decreasing the droplet size, and hence, the SO₂ removal efficiency is increased, as shown in Figure 6c.

4.3. Experimental and Predicted Results Comparison and Analysis. With $V_L/V_G = 10$ L/m³, the relationship between the SO₂ removal efficiency and gas flow rate are presented in Figure 7. The theoretical model established in this paper predicts that SO₂ removal efficiency decreases with gas flow rate increase. The curve shown in the diagram shows a good agreement with the experimental data. As the gas flow rates are in the range of 0.12–0.36 m³/s (superficial gas velocity in inner cylinder is equal to 1.7–5.1 m/s), the predicted results of SO₂ removal efficiency are 92.64–75.60%; and the experimental points are 91.39, 87.21, 84.37, 77.68, and 73.12%, respectively. By comparison with the results, the relative error is below 3.40%.

From the economic point of view, the liquid–gas ratio, V_L/V_G , has been found to be one of the most important criterions for reporting the absorber performance.²² In practical FGD processes, the value of V_L/V_G can be calculated according to its minimum value, expressed as:

$$\frac{V_L}{V_G} = (1.1 \sim 2.0) \left(\frac{V_L}{V_G} \right)_{\min} \quad (47)$$

For the PCF device, the value of $(V_L/V_G)_{\min}$ was calculated as 7.0 L/m³. The studies were carried out at a fixed gas flow rate and the liquid flow rate was controlled according to the requested V_L/V_G . The relationship between SO₂ removal efficiency and liquid–gas ratio is shown in Figure 8.

As shown in the figure that both the predicted and experimental SO₂ removal efficiencies increase continuously with V_L/V_G increasing in the range of $V_L/V_G < 11$ L/m³. However, when V_L/V_G is more than 11 L/m³, the experimental points increase relaxed and are slower than those of prediction. The reason can be explained as follows: With an increase in the amount of V_L/V_G delivered to the absorber, the gas–liquid interface area and total alkalinity for the absorption of SO₂ increase when the gas flow rate is fixed. Consequently, the SO₂ absorption rate increases, and removal efficiency of SO₂ is enhanced. However, when V_L/V_G is too large, the cohesion of droplets will strengthen, and the effective gas–liquid interface

(22) Hrastel, I.; Gerbec, M.; Stergaršek, A. *Chem. Eng. Technol.* **2007**, *30*, 220–233.

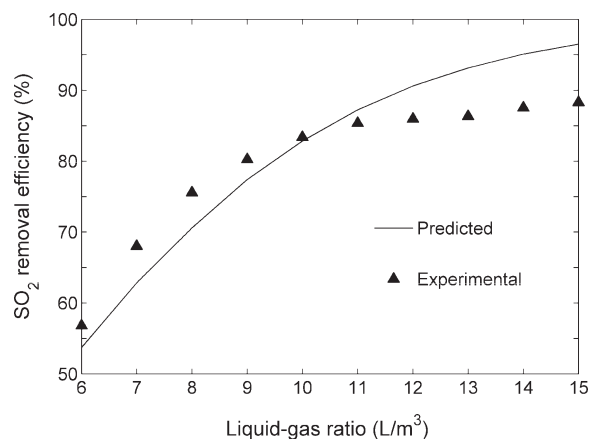


Figure 8. Comparison of SO₂ removal efficiency for different liquid-gas ratios.

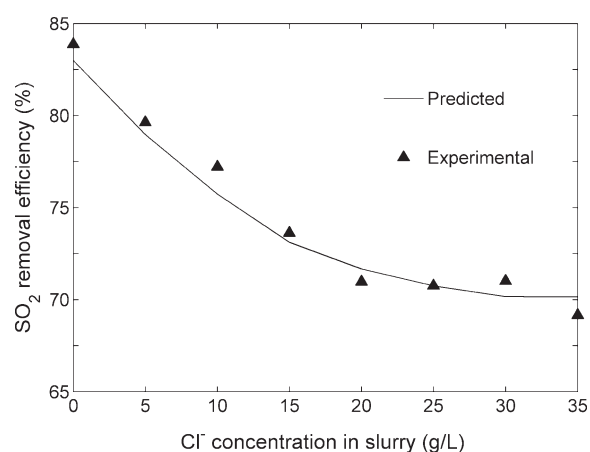


Figure 9. SO₂ removal efficiency for different Cl⁻ concentration.

area no longer increases but even decreases, resulting in smaller volumetric mass-transfer coefficient.²³ This moment, further increase in V_L/V_G becomes meaningless, and the removal efficiency of SO₂ increases relaxed. Because the theoretical model calculates the specific gas-liquid surface area according to eq 31 and cannot reflect the change in the effective gas-liquid interface area, the SO₂ removal efficiency predicted increases continuously and is higher than the experiment's. When the V_L/V_G is controlled in the range of 8–14 L/m³, the relative error is below 8.67%.

4.4. Effects of Cl⁻. The PCF process is a closed-loop desulphurization process. Cl is released during the coal combustion as HCl and can be subsequently absorbed in the slurry. According to Eden and Luckas²⁴ and Frandsen et al.,⁷ the steady-state slurry concentration of Cl⁻ should not exceed 25–30 g/L. Hence, this interval of concentration was studied in the present study. Figure 9 illustrates the results of prediction and experiment. As shown in the figure, the addition of Cl⁻ can strongly affect the desulphurization process. When the Cl⁻ concentration in slurry reaches 25 g/L, SO₂ removal efficiency decreases from 82.99% (83.87%) down to 70.75% (70.75%). The main reason for this effect is assumed to be a decrease in the dissolution rate

of the limestone.^{25–27} When the concentration of Cl⁻ is over 30 g/L, this variation trend become weak. Besides this effect, the Cl⁻ has many other side-effects on the desulphurization system,⁸ such as influencing the dehydration of the desulphurization gypsum, eroding equipments, and reducing the degree of SO₄²⁻ removal. So some measures must be taken to get rid of the Cl⁻ in the desulphurization process.

5. Conclusions

On the basis of the two-film theory, a theoretical model of SO₂ absorption into the droplets of limestone slurry has been developed within the novel wet-type PCF device. The model synthetically considered the purifications of preliminary treating chamber and self-excitation chamber for the SO₂ absorption, and the theoretical SO₂ removal efficiency was compared with the experimental data. The following items were concluded:

(1) Using the two-film theory of gas-liquid mass-transfer, the desulphurization process was analyzed. The results show that, in the ranges of tested operating conditions, the SO₂ absorption rate in preliminary treating chamber (spray zone) is controlled by a combination of gas- and liquid-film diffusions.

(2) Under different operating parameters including the gas flow rate, liquid-gas ratio, and droplet size, the SO₂ absorption rate was analyzed by the model established in this paper. These data indicate that the absorption rate is in direct proportion to the driving force in the range of study. The obtained linear relationships testify to the fact that with the increase of driving force of the absorption process, the value of mass-transfer coefficient does not change with the SO₂ partial pressure.

(3) The gas flow rate, liquid-gas ratio and droplet size all affect, to various extents, the degree of SO₂ removal. The increase of gas flow rate and droplet size, and decrease of liquid-gas ratio all can lead to a decrease of the SO₂ removal efficiency. By comparing the results of prediction and experiment, the data show a good agreement. With $d_p = 2500 \mu\text{m}$, the relative differences of the SO₂ removal efficiency between the predicted and experimental data are below 3.40% and 8.67%, respectively. It demonstrates that the model proposed in present study is an effective model to evaluate and predict the desulphurization performance of the novel PCF device. Moreover, the theoretical model can be extended to apply in other wet FGD technologies.

(4) The addition of Cl⁻ decreased the SO₂ removal efficiency significantly. When the Cl⁻ concentration in slurry reaches 25 g/L, the overall desulphurization efficiency decreased from 83.87 to 70.75%.

(5) Although there is no demister in the PCF device, no water was observed in outlet flue gas during the experiments, showing that the PCF device possesses a good dewatering performance. Meanwhile, no demister means lower energy-consumption, cost, and maintenance.

Acknowledgment. The authors gratefully acknowledge the financial support of the National Natural Science Foundation Project of China (no. NSFC-50878080) and the Key Scientific and Technological Special Project of Changsha City in China (no. K0902006-31).

Supporting Information Available: A list of the nomenclature is provided. This material is available free of charge via the Internet at <http://pubs.acs.org>.

(23) Wu, Y.; Li, Q.; Li, F. *Chem. Eng. Sci.* **2007**, *62*, 1814–1824.
 (24) Eden, D.; Luckas, M. *Chem. Eng. Technol.* **1998**, *21* (1), 56–60.
 (25) He, S.; Oddo, J. E.; Tomson, M. B. *J. Colloid Interface Sci.* **1994**, *162* (3), 297–303.

(26) Ukawa, N.; Takashin, T.; Oshima, M. *J. Chem. Eng. Jpn.* **1993**, *26* (1), 112–113.

(27) Davini, P.; Demichele, G.; Ghetto, P. *Fuel* **1992**, *71* (7), 831–834.